J Appl Physiol 109: 1812–1819, 2010.
First published September 23, 2010; doi:10.1152/japplphysiol.00645.2010.

Vortex formation time-to-left ventricular early rapid filling relation: model-based prediction with echocardiographic validation

Erina Ghosh,[2] Leonid Shmuylovich,[3] and Sándor J. Kovács[1,2,3]

[1]*Cardiovascular Biophysics Laboratory, Cardiovascular Division, Department of Internal Medicine, School of Medicine,* [2]*Department of Biomedical Engineering,* [2]*School of Engineering and Applied Science, and* [3]*Department of Physics, College of Arts and Sciences, Washington University, St. Louis, Missouri*

Submitted 10 June 2010; accepted in final form 20 September 2010

Ghosh E, Shmuylovich L, Kovács SJ. Vortex formation time-to-left ventricular early rapid filling relation: model-based prediction with echocardiographic validation. *J Appl Physiol* 109: 1812–1819, 2010. First published September 23, 2010; doi:10.1152/japplphysiol.00645.2010.— During early rapid filling, blood aspirated by the left ventricle (LV) generates an asymmetric toroidal vortex whose development has been quantified using vortex formation time (VFT), a dimensionless index defined by the length-to-diameter ratio of the aspirated (equivalent cylindrical) fluid column. Since LV wall motion generates the atrioventricular pressure gradient resulting in the early transmitral flow (Doppler E-wave) and associated vortex formation, we hypothesized that the causal relation between VFT and diastolic function (DF), parametrized by stiffness, relaxation, and load, can be elucidated via kinematic modeling. Gharib et al. (Gharib M, Rambod E, Kheradvar A, Sahn DJ, Dabiri JO. *Proc Natl Acad Sci USA* 103: 6305–6308, 2006) approximated E-wave shape as a triangle and calculated VFT_{Gharib} as triangle (E-wave) area (cm) divided by peak (Doppler M-mode derived) mitral orifice diameter (cm). We used a validated kinematic model of filling for the E-wave as a function of time, parametrized by stiffness, viscoelasticity, and load. To calculate $VFT_{kinematic}$, we computed the curvilinear E-wave area (using the kinematic model) and divided it by peak effective orifice diameter. The derived VFT-to-LV early rapid filling relation predicts VFT to be a function of peak E-wave-to-peak mitral annular tissue velocity (Doppler E′-wave) ratio as $(E/E')^{3/2}$. Validation utilized 262 cardiac cycles of simultaneous echocardiographic high-fidelity hemodynamic data from 12 subjects. VFT_{Gharib} and $VFT_{kinematic}$ were calculated for each subject and were well-correlated ($R^2 = 0.66$). In accordance with prediction, $VFT_{kinematic}$ to $(E/E')^{3/2}$ relationship was validated ($R^2 = 0.63$). We conclude that $VFT_{kinematic}$ is a DF index computable in terms of global kinematic filling parameters of stiffness, viscoelasticity, and load. Validation of the fluid mechanics-to-chamber kinematics relation unites previously unassociated DF assessment methods and elucidates the mechanistic basis of the strong correlation between VFT and $(E/E')^{3/2}$.

echocardiography; diastolic function; kinematic modeling; E/E′

THE ABILITY TO QUANTIFY diastolic function (DF) is important in diagnosing heart failure with normal ejection fraction or diastolic heart failure (11, 41). Various approaches to model DF have been proposed, including ones involving fluid mechanics. An index based on this approach to quantify filling efficiency is vortex formation time (VFT) (29). VFT is a dimensionless measure of the time needed for optimal vortex ring formation (18). Gharib et al. (17) defined VFT as the ratio of the velocity of transmitral flow to the orifice diameter integrated over the duration of flow (see APPENDIX B, *Eq. B2*). In vitro values of VFT have been calculated using a left heart flow simulator (17). However, calculating VFT as defined above using clinical data is challenging, and hence approximations are applied. Gharib et al. (9), for example, approximated both early transmitral flow velocity (Doppler E-wave) and the effective orifice diameter as having constant values. Although these approximations allow for clinical estimation of VFT, valuable physiological information may be lost in the process.

An alternate approach for DF quantification involves kinematic modeling of the filling process. This is available via the parametrized diastolic filling (PDF) formalism (19), which has elucidated and characterized new relationships in the physiology of diastole (20). It has been validated in a broad range of clinical applications (32, 34, 21, 33, 28, 38). The PDF formalism accounts for suction-initiated filling and generates accurate Doppler E-wave contours mathematically parametrized by lumped chamber attributes corresponding to load, stiffness, and viscosity/relaxation.

In diastole, chamber wall relaxation unmasks stored elastic strain, allowing the left ventricle (LV) to recoil and act as a suction pump (37) by aspirating blood into the ventricle. Therefore, filling LV relaxation and recoil are closely coupled. Hence, we hypothesized that VFT calculated by fluid mechanics and kinematic approaches should be equivalent. The specific mathematical expression relating VFT to chamber stiffness, relaxation, and load parameters encountered clinically has not been previously determined. Thus we have derived the closed-form mathematical expression for VFT using the PDF model. Validation consists of determining the linear correlation between $VFT_{kinematic}$ and VFT_{Gharib} using human in vivo data. We have shown that the derived expression provides new mechanistic insight into the physiological determinants of VFT and revealed that VFT and the ratio of peak E-wave velocity to peak mitral annular E′-wave peak (E/E′) are directly related (27).

METHODS

Inclusion criteria. We selected 12 datasets from the existing Cardiovascular Biophysics Laboratory database of simultaneous Doppler echocardiographic transmitral flow and micromanometric catheter LV pressure recordings obtained during elective diagnostic cardiac catheterization. Before data acquisition, subjects provided signed, informed consent for participation in accordance with Washington University Human Research Protection Office criteria. All the subjects had normal ejection fraction (EF; 74 ± 6%) (Table 1). Among these 12 datasets, 6 datasets had end-diastolic pressure (LVEDP) < 15 mmHg, 3 datasets had 15 mmHg < LVEDP < 20 mmHg, and 3 datasets had LVEDP > 20 mmHg. The data selection criteria included the presence of normal sinus rhythm, normal valvular function, and

Address for reprint requests and other correspondence: S. J. Kovács, Cardiovascular Biophysics Laboratory, Washington Univ. Medical Center, 660 South Euclid Ave. Box 8086, St. Louis, MO 63110 (e-mail: sjk@wuphys.wustl.edu).

Table 1. *Subject demographics*

	Parameters
No. of Subjects	12 (6 females, 6 males)
Age, yr	56 ± 12
Weight, lb	178 ± 40
Systolic pressure, mmHg	137 ± 28
EF, %	74 ± 6
LVEDP, mmHg	16 ± 3

Values are means ± SD. EF, ejection fraction; LVEDP, left ventricular end-diastolic pressure.

clearly identifiable Doppler E- and A-waves (early and late transmitral flow velocity) and Doppler E′- and A′-waves (early and late mitral annular tissue velocity). A total of 262 cardiac cycles of simultaneous echocardiographic high-fidelity hemodynamic data were analyzed.

Doppler data acquisition. The method of simultaneous echocardiographic transmitral flow and pressure-volume data recording has been previously detailed (22) and is reviewed in APPENDIX A. Our echocardiographic data acquisition methodology was performed in accordance with published American Society of Echocardiography (ASE) criteria (30). Briefly, immediately before catheterization, patients were imaged in a supine position using a Philips iE33 system. Two-dimensional images in apical two- and four-chamber views were obtained. In accordance with convention, the apical four-chamber view was used for Doppler E-wave recording with the sample volume located at the leaflet tips. For E′-wave recording, the lateral aspect of the mitral annulus was chosen. This site was selected because recent studies (30) have shown that in patients with normal EF, E′ data recorded from the lateral aspect of the annulus have the best correlations with LV filling pressures and invasive indices of LV stiffness. We also recorded Doppler M-mode images using the parasternal short-axis view for determination of annular diameter.

Data analysis. In accordance with convention, Doppler E-waves were first approximated as triangles. Duration of the E-wave (E_{dur}) and peak E-wave velocity (E_{peak}) were determined manually using standard criteria (7). The same analysis was applied to tissue Doppler E′-waves. The peak mitral leaflet separation was measured in accordance with Gharib et al. (9) as the maximum separation between the leaflets in M-mode images. The epicardial dimension was also measured from the M-mode images using the method described by Foppa et al. (8).

In addition, we computed the PDF formalism-determined kinematic parameters for each Doppler E- and E′-wave. A model-based image processing algorithm (see APPENDIX A) was applied to E- and E′-waves to generate PDF parameters for the E-wave (c, k, x_o) and the E′-wave (c', k', x'_o) (12, 13, 19, 22, 35).

Since echocardiographic imagers do not simultaneously record E- and E′-waves, we matched E- and E′-waves having the same R-R interval (±15 ms) to calculate E/E′ values for each subject. We analyzed an average of 22 beats from each dataset. Although all the beats were acquired with the patients in a resting state (i.e., similar loading conditions), physiological beat-to-beat variation in wave amplitude and duration was observed, as expected. This resulted in beat-to-beat variation of the parameters (for example, the standard deviation of peak E′-wave velocity, E'_{peak}, was 124.8% of the mean). We therefore averaged the parameters over multiple (~22) beats in each subject so that the effect of physiological beat-to-beat respiratory variation was accounted for, yielding a robust value for E/E′, VFT, and other parameters.

Calculation of VFT_{Gharib}. VFT_{Gharib} was calculated according to *Eq. B3* (see APPENDIX B for details). The parameters were measured from Doppler transmitral flow images by approximating the E-waves as a triangle. This is detailed in APPENDIX A. Peak mitral valve leaflet tip separation ($D_{M\text{-}mode}$) was determined from M-mode images.

Derivation and calculation of the effective mitral orifice diameter. The total four-chambered heart volume remains constant (~95%) during the cardiac cycle. Accordingly, the left heart (atrium + ventricle) can also be approximated as a constant-volume pump (4). We used this physiological attribute to predict the effective mitral orifice diameter for filling. The derivation is detailed in APPENDIX B. Figure 1 shows the left heart as a cylinder of fixed height and external (epicardial) dimension. In diastole, long-axis LV dimension increases (lengthening of the ventricle) with concurrent increase in the endocardial diameter. The apex remains fixed near the sternum. The endocardial-to-epicardial diameter ratio is related to the rate of lengthening of the ventricle (mitral annulus velocity; tissue Doppler E′-wave)-to-rate of ventricular filling (transmitral flow velocity; Doppler E-wave) ratio. The effective mitral orifice diameter is related to E- and E′-waves according to *Eq. B1*. The estimated effective orifice diameter (D_{est}) was computed using peak E′-wave velocity and E-wave velocity at the time of E'_{peak}.

Derivation and calculation of $VFT_{kinematic}$. We derived the kinematic equivalent of VFT via the PDF formalism. The E-wave velocity-time integral (VTI) was expressed using PDF parameters. Effective flow orifice diameter was computed by incorporating constant volume physiology (*Eq. B1*) relating transmitral flow to annulus velocity. The resulting expression for $VFT_{kinematic}$ is given by *Eq. B4*. Validation involved determining the correlation of $VFT_{kinematic}$ to VFT_{Gharib} using in vivo data.

Derivation of relation between VFT and E/E′. The near constant-volume physiological attribute (*Eq. B1*) of the left heart requires that the relationship between effective flow orifice dimension and epicardial dimension be proportional to (E/E′). The final mathematical result in APPENDIX B reveals that VFT is proportional to $(E/E')^{3/2}$. We tested this prediction by determining the correlation of $VFT_{kinematic}$ and VFT_{Gharib} to $(E/E')^{3/2}$.

Numerical and statistical analysis. A MATLAB program (MATLAB 6.0; MathWorks, Natick, MA) was used to determine a triangle fit to Doppler E- and E′-waves. As in previous work (13, 27), we used a model-based image processing program to compute PDF parameters (see APPENDIX A). $VFT_{kinematic}$ and VFT_{Gharib} values were computed for each subject using a custom MATLAB program. Data from multiple beats for each subject were averaged to determine VFT and E/E′ values. Regression analysis was performed to validate the relationship between $VFT_{kinematic}$ and VFT_{Gharib} and both the VFTs and $(E/E')^{3/2}$. The average values were correlated, and Pearson's product moment correlation coefficient (R^2) for each linear regression was determined.

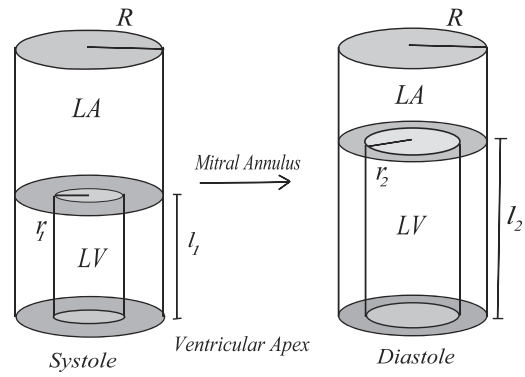

Fig. 1. Schematic diagram of the left heart at end systole and end diastole illustrating its constant-volume property throughout the cardiac cycle. LA, left atrium; LV, left ventricle; R, fixed epicardial radius; r_1, endocardial radius at end systole; r_2, endocardial radius at end diastole' l_1, ventricular long-axis dimension at end systole, l_2, ventricular long-axis dimension at end diastole. Effective mitral orifice co-moving with mitral annulus was omitted for clarity. See text and Ref. 27 for details.

Table 2. *Peak mitral leaflet separation, epicardial diameter, $VFT_{kinematic}$, VFT_{Gharib}, and E/E′ measured and calculated for each of the 12 subjects*

Subject	Mitral Leaflet Separation, cm	Epicardial Diameter, cm	$VFT_{kinematic}$	VFT_{Gharib}	E/E′	Average E-Wave Velocity, cm/s	Average E′-Wave Velocity, cm/s
1	3.1	6.6	1.79	2.49	2.33	59	24
2	3.1	6.1	2.17	3.23	2.33	67	28
3	2.5	6.0	3.94	3.84	5.50	71	13
4	2.8	6.1	4.05	4.56	4.42	71	16
5	3.0	7.2	3.33	3.93	4.89	77	27
6	2.8	7.6	2.51	2.60	7.25	50	7.3
7	2.7	6.5	3.32	3.76	5.27	70	13
8	2.7	6.5	5.32	4.26	10.0	80	8.8
9	2.3	6.2	3.35	3.86	6.36	55	9.0
10	3.4	6.2	3.33	3.08	4.59	68	14
11	2.7	6.6	4.86	3.87	11.8	68	6.2
12	3.0	9.2	4.61	4.74	9.32	89	9.2

Values are peak mitral leaflet separation and epicardial diameter were measured from M-mode images for each of the 12 subjects. For each subject, the kinematic equivalent of vortex formation time ($VFT_{kinematic}$), the VFT determined by Gharib (VFT_{Gharib}), and the ratio of peak E-wave to peak mitral annular tissue velocity (Doppler E′-wave) (E/E′) were calculated over multiple beats, and the averaged value is shown for each subject.

RESULTS

We measured the peak mitral leaflet separation and epicardial diameter from M-mode images and calculated VFT_{Gharib}, $VFT_{kinematic}$, and E/E′ for all data sets as described in METHODS; the values are listed in Table 2. The VFT_{Gharib} values calculated ranged from 2.5 to 4.7 (3.9 ± 0.7).

Validating the derivation of $VFT_{kinematic}$. We validated $VFT_{kinematic}$ by computing the regression relation between VFT_{Gharib} and $VFT_{kinematic}$. The regression relationship obtained was: $VFT_{kinematic} = 1.22(VFT_{Gharib}) - 0.96$, $R^2 = 0.66$. Figure 2 shows $VFT_{kinematic}$ vs. VFT_{Gharib} for data obtained from 12 data sets with the regression line. The values of $VFT_{kinematic}$ ranged from 1.8 to 5.3 (4.3 ± 0.8) (Table 2).

Analysis of the differences between the two components of $VFT_{kinematic}$ vs. VFT_{Gharib}. To understand the differences in the two VFTs, we compared the two methods for calculating the E-wave area and the two methods for calculating the effective flow orifice diameter. The regression relation between the estimated orifice diameter (from the constant-volume attribute) and the measured peak leaflet separation (from M-mode images) was $D_{est} = 1.32$(peak leaflet separation) − 0.01, $R^2 = 0.35$. Figure 3*A* shows the plot of measured leaflet separation vs. estimated diameters for 12 subjects. We also calculated the correlation between triangle-approximated E-wave area and the PDF model-derived E-wave area and found the regression relation to be E-wave area (from integral) =

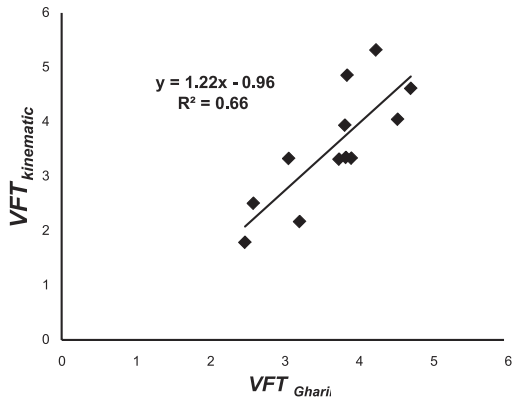

Fig. 2. Validation of the kinematic equivalent of vortex formation time ($VFT_{kinematic}$) as an analog of VFT determined by Gharib et al. (9) by approximating E-waves as a triangle (VFT_{Gharib}). The regression relationship between VFT_{Gharib} and $VFT_{kinematic}$ for 12 subjects is shown. The slope of the regression line (1.22) indicates that $VFT_{kinematic}$ is of the same order of magnitude as VFT_{Gharib}. See text for details.

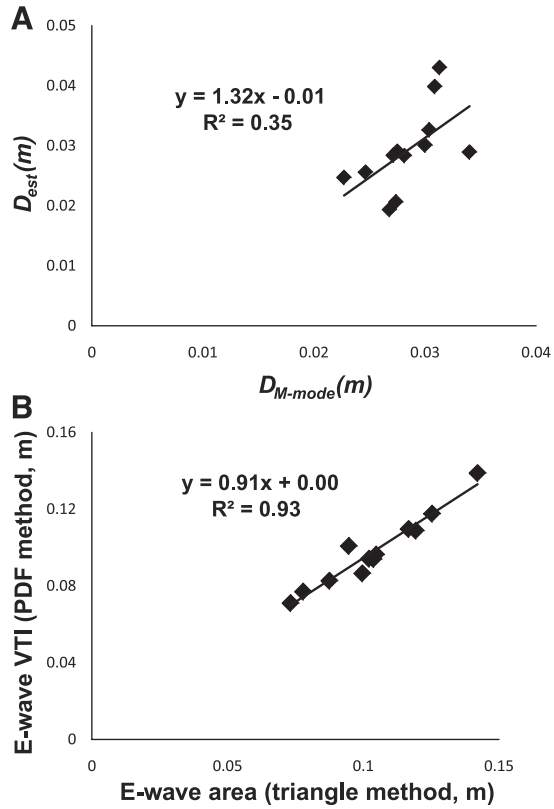

Fig. 3. *A*: comparison of the estimated effective orifice diameter (D_{est}) with the peak mitral leaflet separation ($D_{M\text{-}mode}$). D_{est} is calculated using the constant-volume attribute, and $D_{M\text{-}mode}$ is calculated from M-mode images of LV wall motion. The regression relation shows that the two diameters have the same order of magnitude. *B*: comparison of the E-wave area measured by the triangle method vs. the area calculated by integrating the area under the contour (the E-wave velocity-time integral, VTI). The regression relation indicates that the area calculated using the two methods is similar. See text for details.

0.91(E-wave area) (from triangle), $R^2 = 0.93$. Figure 3*B* shows this relation.

Relationship between VFT and E/E′. In accordance with our mathematical derivation of the relation between VFT and E/E′, we determined the correlation of VFT_{Gharib} (Fig. 4*A*) and $VFT_{kinematic}$ vs. $(E/E')^{3/2}$ (Fig. 4*B*). $VFT_{kinematic}$ correlated with E/E′ according to $VFT_{kinematic} = 0.07[(E/E')^{3/2}] + 2.33$, $R^2 = 0.63$. The regression relation between VFT_{Gharib} and $(E/E')^{3/2}$ is given by $VFT_{Gharib} = 0.03[(E/E')^{3/2}] + 3.24$, $R^2 = 0.19$.

DISCUSSION

VFT has been previously derived using a fluid mechanics-based approach and shown to be an index of diastolic function and cardiac health (9). To further elucidate and characterize the relationship between chamber physiology and VFT, we derived an alternate expression for VFT using a kinematic modeling-based approach. Since ventricular tissue relaxation and recoil generates the atrioventricular pressure gradient, which drives transmitral flow, we hypothesized that a causal connection exists between chamber kinematics and VFT. Accordingly, we derived a kinematic expression for VFT and validated it by comparing $VFT_{kinematic}$ with VFT_{Gharib}, as computed by Gharib's methodology, in the same subjects. Furthermore, the derived mathematical expression for $VFT_{kinematic}$ provided novel mechanistic insight by elucidating the relationship between VFT and E/E′, an established DF index.

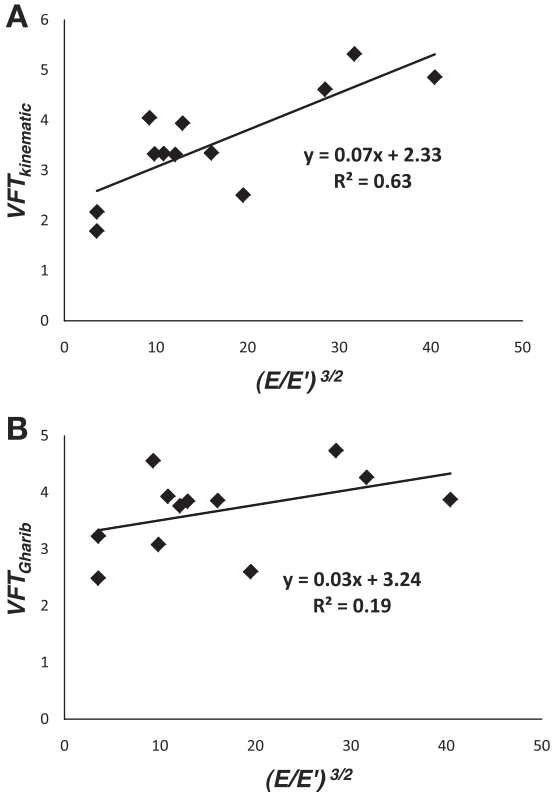

Fig. 4. *A*: correlation of $VFT_{kinematic}$ to $(E/E')^{3/2}$ for all 12 subjects, where E/E′ is the ratio of peak E-wave to peak mitral annular tissue velocity (Doppler E′-wave). The correlation coefficient obtained for this relation was $R^2 = 0.63$. *B*: correlation of VFT_{Gharib} to $(E/E')^{3/2}$ for all 12 subjects. The correlation coefficient obtained for this relation was $R^2 = 0.19$. See text for details.

Insight and background related to vortex rings. Insight into the mathematical connection between chamber kinematics and VFT requires consideration of the physics of vortex rings. When a stream of fluid is injected into a large static fluid volume whose boundary is far removed, at a certain distance from the nozzle a vortex ring develops and grows (10, 23, 29, 39). Its features and temporal evolution depend on fluid properties (usually assumed to be ideal), the geometry (flow orifice size), and the dynamics (injection velocity). For certain parameters, the stream forms a single, growing vortex; for other parameter values, a series of vortices that peel off the injected fluid column can form (10). The opportunity for optimization between the dynamic boundary of the receiving, suitably shaped, fluid chamber (LV chamber) and the entering fluid column (Doppler E-wave) with fluid mechanics-determined vortex ring formation can therefore be immediately appreciated (9, 31).

Indeed, vortex ring formation in the mammalian LV during the early rapid filling phase of diastole (Doppler E-wave) has been studied both theoretically (6, 10, 39, 23, 29, 31) and experimentally (17, 18, 14). Vortex ring formation has both biological/physiological and mechanical consequences. The physiological advantage is that the vortex ring "rinses" the highly trabeculated endocardial surface, preventing thrombus formation associated with stasis of blood, and facilitates mitral leaflet coaptation before systole. The mechanical advantages of vortex formation include redirection of flow to optimize ejection and minimizing fluid stream collision (14), thereby avoiding excessive dissipation of fluid energy, enhancing simultaneous reciprocation of atrial and ventricular volumes during the cardiac cycle in keeping with the near constant-volume property of the four-chambered heart and facilitating efficient contraction (4).

Prior in vitro studies have used LV simulators and prosthetic valves to quantitate vortex formation. Gharib et al. (9) have calculated VFT using traditional approaches (*Eq. B3*) to clinical echo data and found an optimum range of VFT values for normal human hearts. Other groups have used Gharib's method to calculate VFT and found reduced VFT in the setting of reduced systolic function (15, 16) and reduced VFT in patients with Alzheimer's disease (36).

Connecting kinematics and vortex ring formation. To appreciate the causal relation between VFT and the physiological DF determinants, we derived VFT using a kinematic model of filling. The motivation behind deriving VFT using kinematics is to elucidate and characterize the coupling between chamber properties (stiffness, relaxation) and fluid flow. The kinematic approach characterizes filling in terms of load, stiffness, and relaxation/viscosity, familiar to physiologists and cardiologists. Therefore, $VFT_{kinematic}$ complements and advances our understanding of the proper way to interpret VFT_{Gharib}. *Equation B4* expresses $VFT_{kinematic}$ in terms of the PDF parameters k, c, and x_o, which have established physiological analogs (2, 19, 22, 26).

The regression value of the VFT_{Gharib} vs. $VFT_{kinematic}$ relation ($R^2 = 0.66$) validates our prediction that $VFT_{kinematic}$ is analogous to VFT_{Gharib}. The slope of the regression relation (1.22) indicates that the two VFTs are of similar magnitude, further validating the functional equivalence of the two expressions.

Understanding the differences in computing $VFT_{kinematic}$ vs. VFT_{Gharib}. The correlation between $VFT_{kinematic}$ and VFT_{Gharib} indicates that although these two parameters are similar, they are not equivalent. The key to understanding the differences between them is in the approximations used in their determination. VFT_{Gharib} applies two major approximations: *1*) a constant effective mitral valve orifice area and *2*) a constant inflow velocity. $VFT_{kinematic}$ also employs approximations, but these are mitigated by key physiological principles. $VFT_{kinematic}$ treats the time-varying E-wave as a time-varying inflow velocity in accordance with the PDF model. In addition, $VFT_{kinematic}$ incorporates the near "constant-volume property" of the left heart for effective orifice area estimation, thereby providing a more physiologically realistic estimate than M-mode obtained at a single instant of filling.

Since computing VFT from *Eq. B2* is not feasible, our approximations enable us to calculate VFT from routine clinical data. The different type of approximations used in $VFT_{kinematic}$ vs. VFT_{Gharib} is the reason why the two VFTs are not equivalent. In addition, there are practical limitations in acquiring data in a clinical setting. (See *Limitations*) Hence, the very good correlation observed between the two VFTs is reassuring.

The differences in the definition of $VFT_{kinematic}$ from VFT_{Gharib} arise from the method used to calculate the E-wave area and the effective mitral orifice diameter. To understand how much each of these terms differed, we compared the values of D_{est} (from the constant-volume attribute) with those of $D_{M\text{-}mode}$ in Fig. 3*A* and with the E-wave area, calculated using the two different methods, in Fig. 3*B*. Figure 3*B* indicates that E-wave area calculated by approximating it as a triangle is nearly equivalent to the area obtained by integration. Hence, observed differences in VFT arise from the differences in how effective mitral orifice diameter is approximated.

The correlation between D_{est} and $D_{M\text{-}mode}$ is modest as expected ($R^2 = 0.35$; Fig. 3*A*) because of the inherent limitation in measurement of leaflet separation due to transducer position and angulation relative to LV long-axis direction. VFT_{Gharib} incorporates $D_{M\text{-}mode}$ measured using M-mode echo, and hence it is subject to the same limitations. The measurement of epicardial dimension (for calculating D_{est}) is subject to the same challenges as well. To mitigate the effect of this limitation, we incorporated constant-volume physiology in effective flow orifice diameter determination. This effectively reduces the sensitivity of the D_{est} to measurement errors while incorporating physiology. Our method of effective flow orifice diameter calculation is further validated by the slope (1.32) in Fig. 3*A*, indicating that D_{est} and $D_{M\text{-}mode}$ are of similar order of magnitude.

New insight into physiology of filling: relation to E/E′. The derivation of $VFT_{kinematic}$ also sheds light on the relationship between VFT and E/E′. Since the near constant-volume physiology relates effective flow orifice diameter to this ratio, $VFT_{kinematic}$ is a function of E/E′. A more detailed analysis shows that VFT is proportional to $(E/E')^{3/2}$. This dependence is explained in detail in APPENDIX B.

The VFT-to-$(E/E')^{3/2}$ relation has clinical implications. E/E′ is a widely used noninvasive DF index (27) since E/E′ alone or in conjunction with other indexes is a correlate of diastolic dysfunction (25). E/E′ has also been shown to be a marker for elevated LVEDP (30). From the physiological perspective, E/E′ reflects the ratio of global (3-dimensional, long-axis + short-axis) relaxation/volume accommodation via the E-wave and longitudinal (1-dimensional) relaxation/volume accommodation via the E′-wave, thereby accounting for the (2-dimensional, i.e., short-axis) radial motion as a result of volume conservation. VFT, incorporating the near constant-volume attribute, encompasses this feature of E/E′, and hence it is sensitive to changes in magnitude of radial accommodation of the E-wave volume. The relationship between VFT and E/E′ has been observed previously (24), but the causal physiology has not been elucidated.

In accordance with prediction, $VFT_{kinematic}$ achieved a correlation of $R^2 = 0.63$ with $(E/E')^{3/2}$ (Fig. 4*A*). VFT_{Gharib} has a lower correlation with $(E/E')^{3/2}$ ($R^2 = 0.19$) (Fig. 4*B*). This result agrees with previous observation (24) and our theoretical prediction. The poor correlation between VFT_{Gharib} and $(E/E')^{3/2}$ is due to the approximations used by VFT_{Gharib}. Our derivation (APPENDIX B) shows that VFT is a correlate of $(E/E')^{3/2}$. The correlation of $VFT_{kinematic}$ to $(E/E')^{3/2}$ validates this in the setting of the approximations made and shows that $VFT_{kinematic}$ is physiologically a more faithful estimate of VFT than VFT_{Gharib}.

We used Fig. 3 to identify the terms that introduce major differences between VFT_{Gharib} and $VFT_{kinematic}$. We concluded that using mitral leaflet separation measured by M-mode echo introduces errors in estimation of effective flow orifice diameter. Hence, using $D_{M\text{-}mode}$ to approximate the effective flow orifice diameter makes VFT_{Gharib} less sensitive to E/E′. When VFT is calculated more physiologically, using a kinematic approach incorporating near constant-volume physiology, the causal E/E′-to-$VFT_{kinematic}$ connection is restored.

Limitations. Because of the format in which E-waves and M-mode data are recorded clinically, computing VFT as defined by *Eq. B2* requires modifications. To derive VFT_{Gharib}, Gharib et al. approximated the Doppler E-wave velocity as a constant during early filling. They also assumed that the effective orifice diameter is constant during early filling.

To calculate the effective mitral orifice diameter (D_{est}), we approximated the left heart as a constant-volume cylinder. This model incorporates longitudinal motion and concomitant wall thinning as the only degree of freedom for incoming volume accommodation. In the in vivo setting for a normal ventricle, blood is accommodated primarily by longitudinal elongation and also by slight (epicardial) radial expansion, the "crescent effect" (40). Hence the near constant-volume approximation has slight limitations. However, use of the constant-volume approximation for the left heart is legitimized by its ability to provide effective mitral orifice diameter at E'_{peak}, when volume accommodation is primarily due to longitudinal elongation.

In deriving $VFT_{kinematic}$, we assumed simultaneous E- and E′-wave onset. It is possible that some E-waves are slightly delayed (by a few milliseconds) beyond E′-wave onset. To determine whether the assumption of E- and E′-wave nonsimultaneity influences the value of VFT, we defined a time-delay constant and performed numerical experiments. We then plotted the relationship between VFT and the time-delay constant and found insignificant variation in VFT. Thus the assumption that E′- and E-waves have simultaneous onset is warranted.

The machine imposed limitation of nonsimultaneous E- and E′-wave recording was handled by selecting matched E- and E′-waves with R-R intervals within ±15 ms of each other. Since all the cardiac cycles analyzed had diastasis, the minor difference in R-R intervals only affects diastasis duration rather than the E- or the E′-wave duration (4). Hence, our method is limited to E- and E′-waves with a clear diastatic interval.

In accordance with convention (10), we used Doppler M-mode in the parasternal short-axis view for $D_{\text{M-mode}}$ and epicardial dimension determination. Although M-mode echo may underestimate (1) mitral leaflet separation and epicardial dimension, using the same recording method in all subjects is a systematic effect and should apply to all VFT values equally. We also assume that the maximum mitral effective flow orifice diameter occurred at the peak of the E′-wave during the cardiac cycle.

This study aims to understand VFT in the context of a range diastolic function with normal systolic function. Hence, we restricted our analysis to subjects with normal EF but a range of LVEDP encountered clinically. However, for VFT to achieve broader clinical use, further application in a more diverse population with a larger variation in EF and systolic function is justified.

Conclusions. Vortex formation time ($\text{VFT}_{\text{Gharib}}$) is a fluid mechanics-derived index reflecting optimum vortex formation and diastolic filling efficiency. Incorporating near constant-volume (left heart) physiology and chamber kinematics, we derived $\text{VFT}_{\text{kinematic}}$, the analog of $\text{VFT}_{\text{Gharib}}$. Validation utilized simultaneous echocardiography-catheterization data from 12 patients with normal EF and varying EDP. Excellent correlation between $\text{VFT}_{\text{kinematic}}$ and $\text{VFT}_{\text{Gharib}}$ ($R^2 = 0.66$) was observed. The derivation of $\text{VFT}_{\text{kinematic}}$ revealed it to be a function of $(\text{E/E}')^{3/2}$, whose observed correlation ($R^2 = 0.63$) using in vivo human data further validated the new relationship. $\text{VFT}_{\text{kinematic}}$ provides physiological and mechanistic insight into the coupling between transmitral flow and chamber properties. Further application and validation in additional, well-defined clinical subsets is warranted.

APPENDIX A

Simultaneous acquisition of echocardiographic and high-fidelity hemodynamic data. Before arterial access, in the catheterization laboratory, a full two-dimensional echo-Doppler study is performed by an ASE-certified sonographer in accordance with ASE criteria (30). After appropriate sterile skin prep and drape, local anesthesia (1% Xylocaine) is given and percutaneous right or left femoral arterial access is obtained in preparation for catheterization and angiography, using a valved sheath (6-F; Arrow, Reading, PA). After arterial access and placement of a 64-cm sheath (Arrow), a 6-F micromanometer-tipped pigtail (triple pressure transducer) pressure-volume conductance catheter (model 560-1, 560-5; Millar Instruments, Houston, TX) is directed into the mid-LV in a retrograde fashion across the aortic valve under fluoroscopic control. Before insertion, the manometer-tipped catheter is calibrated against "zero" by submersion just below the surface of a normal saline bath at 37°C and again after insertion relative to hydrostatic "zero" using the lumen with respect to the midthoracic fluid-filled transducer (HP). It is balanced using a transducer control unit (model TC-510; Millar Instruments), and pressures are fed to the catheterization laboratory amplifier (Quinton Diagnostics, Bothell, WA or GE Healthcare, Milwaukee, WI) and simultaneously into the input ports of the physiological amplifier of the Doppler imaging system for synchronization (Philips iE33). With the patient supine, apical four-chamber views using a 2.5-MHz transducer are obtained by the sonographer, with the sample volume gated at 1.5–5 mm directed between the tips of the mitral valve leaflets and orthogonal to the mitral valve plane. Continuous wave Doppler is used to record aortic outflow and mitral inflow from the apical view for determination of the isovolumic relaxation time (IVRT) using a sweep speed of 10 cm/s. Doppler tissue imaging (DTI) of the medial and the lateral mitral annulus and M-mode images are also recorded. The method for DTI has been described previously (35). DTI was performed at a sample size gated at 2.5 mm for most of the subjects and positioned at the lateral site of the mitral annulus. To synchronize the hemodynamic data with the Doppler data, a fiducial marker in the form of a square wave is fed from the catheter-transducer control unit. The LV and aortic pressures, LV volume from the conductance catheter, and one ECG channel are also simultaneously recorded on disk. Simultaneous Doppler data, LV pressure, and conductance volume are obtained for a minimum of 30 consecutive beats during quiet respiration. After data acquisition, the diagnostic catheterization procedure is performed in the usual manner.

PDF formalism. At mitral valve opening, LV pressure continues to decrease while LV volume increases, thereby initiating filling via mechanical suction of atrial blood. Suction-initiated filling has been modeled kinematically using the PDF formalism, which characterizes the kinematics in analogy to the recoil from rest of a previously displaced, damped simple harmonic oscillator (SHO). The motion is parametrized by k, the spring constant (LV chamber stiffness); c, the damping constant (chamber relaxation/viscoelasticity); and x_o, the initial SHO displacement (volumetric load). These parameters are uniquely determined for each beat by using a model- based image processing program to solve the "inverse" problem. The digitized clinical E-wave contour is the input, and the model parameters are the best-fit (Levenberg-Marquardt) determined output. Most clinical E-wave contours (cm/s) can be fit by solutions in the "underdamped" regime ($c^2 < 4k$) of motion given by

$$\text{E}(t) = -\frac{kx_o}{\omega}\sin \omega t \cdot e^{-ct/2} \qquad (A1)$$

where $\omega = 4k - c^2/2$. This solution and the "overdamped" kinematic regime ($c^2 > 4k$) solution provides an excellent fit to all clinically encountered E-waves.

The PDF formalism is also used to characterize DTI determined E′-wave. During filling, the annulus moves toward the atrium, allowing longitudinal elongation of the ventricle according to the rules of harmonic oscillatory motion. Thus E′-wave velocity is characterized by three SHO parameters: k', c', and x'_o. By analogy, the equation for E′-wave velocity in the underdamped regime is

$$\text{E}'(t) = -\frac{k' x'_o}{\omega'}\sin \omega' t \cdot e^{-c't/2} \qquad (A2)$$

where $\omega' = 4k' - (c')^2/2$. To extract PDF parameters from clinical E- and E′-wave contours, a model-based image processing program is used. The process of fitting has been described in detail previously (12, 13). This method of PDF parameter determination has an inter-observer variability of 8% (3). In this work, underdamped ($4k - c^2 > 0$) E- and E′-waves were selected for analysis.

APPENDIX B

Derivation of effective mitral orifice diameter using constant-volume attribute of the left heart. The total left heart (atrium + ventricle) volume during the cardiac cycle remains nearly constant (4). In diastole, both the short-axis (endocardial-internal chamber dimension) and long-axis dimensions (annular displacement) of the chamber increase while the outer (epicardial) dimension remains essentially fixed and the apex remains spatially fixed in accordance with left heart constant-volume physiology. We used this property to

derive an expression for the effective orifice diameter. To illustrate the constant-volume attribute, a schematic representation of the left heart is shown in Fig. 1. The left heart is approximated as a cylinder of fixed external radius with a time-varying internal radius and height. The ventricular apex, base, and atrium are denoted in Fig. 1. The epicardial radius is R, the endocardial radius at end systole is r_1, and the endocardial radius during diastole is r_2. The long axis of the ventricle is l_1 in systole and l_2 in diastole. From systole to the end of the E-wave, the inner volume (endocardial volume) increases to accommodate filling. The tissue volume remains constant since tissue is incompressible (35). With the use of these two constraints, the effective mitral orifice diameter as a function of time is

$$D_{\text{est}}(t) = D_{\text{epi}}\sqrt{\frac{\mathrm{E}'(t)}{\mathrm{E}(t)}} \tag{B1}$$

In this equation, D_{epi} is the (fixed) epicardial dimension.

Derivation of vortex formation time via kinematics. VFT has been defined by Kheradvar and Gharib (17) as

$$\text{VFT} = \int_0^T \frac{\mathrm{E}(t)}{D(t)}\mathrm{d}t \tag{B2}$$

where $D(t)$ is mitral orifice diameter. To calculate VFT, Gharib et al. (9) approximated $D(t)$ by taking the E-wave velocity averaged over the duration of E-wave, multiplied by the duration of the E-wave and divided by the peak effective mitral flow orifice diameter (taken to be a constant). Since the E-wave is conventionally fit by a triangle, the average E-wave velocity is $E_{\text{peak}}/2$. The duration of E-wave is E_{dur}. This definition of VFT is expressed as $\text{VFT}_{\text{Gharib}}$ and is mathematically defined as

$$\text{VFT}_{\text{Gharib}} = \frac{\mathrm{E}_{\text{peak}} \times \mathrm{E}_{\text{dur}}}{2 \times D_{\text{M-mode}}} \tag{B3}$$

where $D_{\text{M-mode}}$ is the peak mitral leaflet separation.

To derive the kinematic equivalent ($\text{VFT}_{\text{kinematic}}$), we integrated E-wave velocity (*Eq. A1*) over the duration of flow and divided it by D_{est} (*Eq. B1*). Hence the mathematical expression is

$$\text{VFT}_{\text{kinematic}} = \frac{x_o\left[1 + \exp\left(-c\pi/2\omega\right)\right]}{D_{\text{est}}\left(t_{\mathrm{E}'_{\text{peak}}}\right)} \tag{B4}$$

Relationship between VFT and E/E′. The E-wave volume can be approximated as a fluid cylinder whose diameter equals the effective mitral orifice diameter. To appreciate how VFT depends on dimensions of the filling column, consider two ventricles having different effective orifice diameters filling with the same volume (V). The volume for a cylinder of height L and diameter D is $\mathrm{V} = \pi L(D^2/4)$. VFT for the fluid cylinder is defined as

$$\text{VFT} = \frac{L}{D} = \frac{4\mathrm{V}}{\pi D^3} \tag{B5}$$

As the effective mitral orifice diameter decreases for the same E-wave volume, VFT increases as the cube of the diameter. Invoking the constant-volume attribute (*Eq. B1*), VFT becomes

$$\text{VFT} \cong \frac{1}{D^3} = \left(\frac{\mathrm{E}}{\mathrm{E}'}\right)^{3/2} \tag{B6}$$

This analysis is applicable in the setting of essentially similar values for E-wave volume. In the datasets analyzed we found very small variation (the standard deviation in the values was ±7.7 ml) in E-wave volumes among the subjects, thus justifying the derivation in *Eq. B6*.

ACKNOWLEDGMENTS

The assistance of Peggy Brown in expert echocardiographic data acquisition and the assistance of the staff of the cardiac catheterization laboratory at Barnes-Jewish Hospital at Washington University Medical Center are gratefully acknowledged.

GRANTS

This work was supported in part by the Alan A. and Edith L. Wolff Charitable Trust (St. Louis, MO) and the Barnes-Jewish Hospital Foundation. L. Shmuylovich is the recipient of a Heartland Affiliate predoctoral fellowship award from the American Heart Association.

DISCLOSURES

No conflicts of interest, financial or otherwise, are declared by the author(s).

REFERENCES

1. **Anwar AM, Soliman O II, Cate FJ, Nemes A, McGhie JS, Krenning BJ, van Geuns RJ, Galema TW, Geleijnse ML.** True mitral annulus diameter is underestimated by two-dimensional echocardiography as evidenced by real-time three-dimensional echocardiography and magnetic resonance imaging. *Int J Cardiovasc Imaging* 23: 541–547, 2007.
2. **Bauman L, Chung CS, Karamanoglu M, Kovács SJ.** The peak atrioventricular pressure gradient to transmitral flow relation: kinematic model prediction with in-vivo validation. *J Am Soc Echocardiogr* 17: 839–844, 2004.
3. **Boskovski MT, Shmuylovich L, Kovács SJ.** Transmitral flow velocity-contour variation after premature ventricular contractions: a novel test of the load-independent index of diastolic filling. *Ultrasound Med Biol* 34: 1901–1908, 2008.
4. **Bowman AW, Kovács SJ.** Assessment and consequences of the constant-volume attribute of the four-chambered heart. *Am J Physiol Heart Circ Physiol* 285: H2027–H2033, 2003.
5. **Chung CS, Kovács SJ.** Consequences of increasing heart rate on deceleration time, velocity time integral and E/A. *Am J Cardiol* 47: 398–402, 2006.
6. **Dabiri JO.** Optimal vortex formation as a unifying principle in biological propulsion. *Annu Rev Fluid Mech* 41: 17–33, 2009.
7. **Feigenbaum H.** *Echocardiography* (5th ed.). Baltimore, MD: Lea and Febiger, 1994, p. 677.
8. **Foppa M, Duncan BB, Rohde LEP.** Echocardiography-based left ventricular mass estimation. How should we define hypertrophy? *Cardiovasc Ultrasound* 3: 17, 2005.
9. **Gharib M, Rambod E, Kheradvar A, Sahn DJ, Dabiri JO.** Optimal vortex formation as an index of cardiac health. *Proc Natl Acad Sci USA* 103: 6305–6308, 2006.
10. **Gharib M, Rambod E, Shariff K.** A universal time-scale of vortex formation time. *J Fluid Mech* 360: 121–140, 1998.
11. **Gheorghidae M, Pang PS.** Acute heart failure syndromes. *J Am Coll Cardiol* 53: 557–573, 2009.
12. **Hall AF, Aronovitz JA, Nudelman SP, Kovács SJ.** Automated method of characterization of diastolic transmitral Doppler velocity contours: late atrial filling. *Ultrasound Med Biol* 20: 859–869, 1994.
13. **Hall AF, Kovács SJ.** Automated method for characterization of diastolic transmitral Doppler velocity contours: early rapid filling. *Ultrasound Med Biol* 20: 107–116, 1994.
14. **Hong G, Pedrizzetti G, Tonti G, Li P, Wei Z, Kim JK, Baweja A, Liu Chung N S, Houle H, Narula J, Vannan MA.** Characterization and quantification of vortex flow in the human left ventricle by contrast echocardiography using vector particle image velocimetry. *JACC Cardiovasc Imaging* 1: 705–717, 2008.
15. **Jiamsripong P, Calleja AM, Alharthi MS, Cho EJ, McMahon EM, Heys JJ, Milano M, Sengupta PP, Khaderia BK, Belohlavek M.** Increase in late diastolic filling force is associated with impaired transmitral flow efficiency in acute moderate elevation left ventricular afterload. *J Ultrasound Med* 28: 175–182, 2009.
16. **Jiamsripong P, Calleja AM, Alharthi MS, Dzsinich M, McMahon EM, Heys JJ, Milano M, Sengupta PP, Khaderia BK, Belohlavek M.** Impact of acute moderate elevation in left ventricular afterload on diastolic transmitral flow efficiency: analysis by vortex formation time. *J Am Soc Echocardiogr* 22: 427–431, 2009.
17. **Kheradvar A, Gharib M.** On mitral valve and its connection to early diastolic flow. *Ann Biomed Eng* 37: 1–13, 2009.
18. **Kheradvar A, Milano M, Gharib M.** Correlation between vortex ring formation and mitral annulus dynamics during ventricular rapid filling. *ASAIO J* 53: 8–16, 2007.

19. **Kovács SJ, Barzilai B, Pérez JE.** Evaluation of diastolic function with Doppler echocardiography: the PDF formalism. *Am J Physiol Heart Circ Physiol* 252: H178–H187, 1987.
20. **Kovács SJ, Meisner JS, Yellin EL.** Modeling of diastole. In: *Cardiology Clinics*, edited by Crawford MH and Kovács SJ. Philadelphia, PA: Saunders, 2000, p. 459–487.
21. **Kovács SJ, Rosado J, McGuire ALM, Hall AF.** Can transmitral Doppler E-waves differentiate hypertensive hearts from normal? *Hypertension* 30: 788–795, 1997.
22. **Kovács SJ, Sester R, Hall AF.** Left ventricular chamber stiffness from model-based image processing of transmitral Doppler E-waves. *Coron Artery Dis* 8: 179–187, 1997.
23. **Krueger P, Gharib M.** The significance of vortex ring formation to the impulse and thrust of a starting jet. *Phys Fluids* 15: 1271–1281, 2003.
24. **Lee LC, Tan YL, Tan HC, Omar AR, Chai P, Yeo TC, Low AFH, Yip JWL, Chia BL, Poh KK.** Vortex formation index in heart failure: novel non-invasive assessment of fluid dynamics using transthoracic echocardiography (Abstract). *Circulation* 116: II-741, 2007.
25. **Liang HY, Cauduro SA, Pellikka PA, Bailey KR, Grossardt BR, Yang EH, Rihal C, Seward JB, Miller FA, Abraham TP.** Comparison of usefulness of echocardiographic Doppler variables to left ventricular end-diastolic pressure in predicting future heart failure events. *Am J Cardiol* 97: 866–871, 2006.
26. **Lisauskas JB, Singh J, Bowman AW, Kovács SJ.** Chamber properties from transmitral flow: prediction and validation of average and passive left ventricular stiffness. *J Appl Physiol* 91: 154–162, 2001.
27. **Lisauskas JB, Singh J, Courtois MR, Kovács SJ.** The relation of the peak Doppler E-wave velocity to peak mitral annulus velocity ratio in diastolic function. *Ultrasound Med Biol* 27: 499–507, 2001.
28. **Meyer TE, Kovács SJ, Ehsani AA, Klein A, Holloszy JO, Fontana L.** Long-term caloric restriction ameliorates the decline in diastolic function in humans. *J Am Coll Cardiol* 47: 398–402, 2006.
29. **Mohseni K, Gharib M.** A model for universal time scale of vortex ring formation. *Phys Fluids* 10: 2436–2438, 1998.
30. **Nagueh SF, Appleton CP, Gillebert TC, Marino PN, Oh JK, Smiseth OA, Waggoner AD, Flachskampf FA, Pellikka PA, Evangelista A.** Recommendations for the evaluation of left ventricular diastolic function by echocardiography. *J Am Soc Echocardiogr* 22: 107–133, 2009.
31. **Pedrizzetti G, Domenichini F.** Nature optimizes the swirling flow in the human left ventricle. *Phys Rev Lett* 95: 108101-1–108101-4, 2005.
32. **Rich MW, Stitziel NO, Kovács SJ.** Prognostic value of diastolic filling parameters derived using novel image processing techniques in patients ≥70 years of age with congestive heart failure. *Am J Cardiol* 84: 82–86, 1999.
33. **Riordian MM, Chung CS, Kovács SJ.** Diabetes and diastolic function: stiffness and relaxation from the transmitral flow. *Ultrasound Med Biol* 31: 1589–1596, 2005.
34. **Riordian MM, Kovács SJ.** Elucidation of spatially distinct compensatory mechanisms in diastole: radial compensation for impaired longitudinal filling in left ventricular hypertrophy. *J Appl Physiol* 104: 513–520, 2008.
35. **Riordian MM, Kovács SJ.** Quantitation of mitral annular oscillations and longitudinal "ringing" of the left ventricle: a new window into longitudinal diastolic function. *J Appl Physiol* 100: 112–119, 2006.
36. **Roher AE, Belohlavek M, Maarouf CL, Kokjohn TA, Garami Z, Beach TG, Sabbagh MN.** Echocardiography vortex formation time reveal cardiac diastolic transmitral flow dysfunction in Alzheimer's disease patients. *Alzheimers Dement* 5, *Suppl* 1: P293–P293, 2009.
37. **Shmuylovich L, Chung CS, Kovács SJ, Yellin EL, Nikolic SD.** Point: Left ventricular volume during diastasis is the physiological in vivo equilibrium volume and is related to diastolic suction. *J Appl Physiol* 109: 606–608, 2010.
38. **Shmuylovich L, Kovács SJ.** Load independent index of diastolic filling: model-based derivation with in vivo validation in control and diastolic dysfunction subjects. *J Appl Physiol* 101: 92–101, 2006.
39. **Shusser M, Gharib M.** Energy and velocity of a forming vortex ring. *Phys Fluids* 12: 618–621, 1999.
40. **Waters EA, Bowman AW, Kovács SJ.** MRI-determined left ventricular "crescent effect": a consequence of the slight deviation of contents of the pericardial sack from the constant-volume state. *Am J Physiol Heart Circ Physiol* 288: H848–H853, 2005.
41. **Zile MR, Brutsaert DL.** New concepts in diastolic dysfunction and diastolic heart failure: Part I. *Circulation* 105: 1387–1393, 2002.